Stereodynamics of the O(^{3}P) with H_2 (D_2) ($\nu = 0$, $j = 0$) reaction*

Liu Yu-Fang(刘玉芳)†, He Xiao-Hu(和小虎),
Shi De-Heng(施德恒), and Sun Jin-Feng(孙金锋)

Department of Physics, Henan Normal University, Xinxiang 453007, *China*

(Received 16 October 2010; revised manuscript received 4 December 2010)

Quasi-classical trajectory theory is used to study the reaction of O(^{3}P) with H_2 (D_2) based on the ground ^{3}A″ potential energy surface (PES). The reaction cross section of the reaction O+H_2→OH+H is in excellent agreement with the previous result. Vector correlations, product rotational alignment parameters $\langle P_2(\boldsymbol{j}' \cdot \boldsymbol{k})\rangle$ and several polarized-dependent differential cross sections are further calculated for the reaction. The product polarization distribution exhibits different characteristics that can be ascribed to different motion paths on the PES, arising from various collision energies or mass factors.

Keywords: quasi-classical trajectory method, O+H_2 reaction, reaction cross section, vector correlation

PACS: 82.20.Bc, 31.15.xv, 34.50.Lf **DOI:** 10.1088/1674-1056/20/7/078201

1. Introduction

The reaction O(^{3}P)+H_2 and its isotopic variants are of fundamental significance in chemical dynamics and have been the subject of extensive experimental and theoretical studies for decades because of their role in combustion processes[1] and atmospheric chemistry.[2] Theoretical investigations are important because this is the simplest reaction involving oxygen atoms and is a typical hydrogen abstraction reaction. Many results and properties of the reaction have been obtained experimentally over a wide range.[3−5] However, because any source of O(^{3}P) atoms has a tiny number ($\sim 10^{-6}$) of O(^{1}D) atoms and the reaction cross section of O(^{3}P)+H_2 is six orders of magnitude[6] or above smaller than that of O(^{1}D)+H_2 at low energy ($\sim$0.5 eV), experimental investigations of reactions with O(^{3}P) atoms are difficult. Thus, theoretical studies on this reaction are preferred.

Several typical theories have been used to calculate the reaction O(^{3}P)+H_2 →OH+H, including quasi-classical trajectory theory,[7] transition state theory[8] and quantum mechanical theory.[9−11] Previous studies on the O(^{3}P)+H_2 reaction have dealt with several scalar properties such as the thermal rate coefficient and the isotope effects,[12−14] the reactive cross section,[5,11,13,15] the reaction probability[16,17] and the effects of the ro-vibrational energy distribution.[4,12] A variety of potential energy surfaces (PESs) have been applied to the calculation of the O(^{3}P)+H_2 reaction, and made excellent and significant achievements.[9,13,18−20] Rogers *et al.*[18] calculated the electronic energies of the lowest ^{3}A′ and ^{3}A″ states of the O(^{3}P) + H_2 system using MOLPRO and fitted two PESs for these two states.[18] Brandão *et al.* [19]reported a new potential energy surface for the O(^{3}P)+H_2 system on the lowest ^{3}A″ state built using *ab initio* data calculated by Rogers *et al.*

For a complete theoretical study of the dynamics of a reaction, both the vector and scalar properties should be considered. Stereodynamics can provide a great deal of vector information about a reaction that cannot be obtained if only the scalar properties are considered.[21,22] To gain a better understanding of the dynamics of the title reaction, we use the quasi-classical trajectory (QCT) theory to calculate the stereodynamics on a PES of the ground ^{3}A″ electronic state reported by Brandão *et al.*[19] The reaction cross section is also calculated as a function of the collision energy for comparison with QCT results[11] and quantum results.[5,13]

*Project supported by the National Natural Science Foundation of China (Grant Nos. 60977063 and 10574039) and the Innovation Scientists and Technicians Troop Construction Projects of Henan Province of China (Grant No. 084100510011).

†Corresponding author. E-mail: yf-liu@henannu.edu.cn

© 2011 Chinese Physical Society and IOP Publishing Ltd

2. Calculations

Theoretical details of the QCT method are reported elsewhere.[20,22−28] The Hamilton equations are numerically integrated in three dimensions. The initial vibrational and rotational quantum numbers are taken as $\nu = 0$ and $j = 0$, respectively. Batches of 10,000 trajectories are run for each reaction energy in calculating the reaction cross section and rotational polarization parameters for an integration step of 0.1 fs, which guarantees the conservations of total energy and total angular momentum. Beside these calculations, batches of 50,000 trajectories are run for the reaction $O(^3P)+H_2 \rightarrow OH+H$ at collision energies of 0.55, 1.0, 1.5, and 3.0 eV separately. Low collision energy (0.55 eV) is close to the energy in the van der Waals region, and high collision energies (1.0, 1.5, and 3.0 eV) are far from van der Waals region. The calculations at those collision energies reflect dynamic properties of this reaction more preferably. The reaction cross section is defined as $\sigma_r = \pi b_{max}^2 (N_r/N)$, where N_r is the number of reactive trajectories and N is the number of total trajectories. The sampling error is defined as $\varepsilon = \sqrt{(N - N_r)/NN_r} \times 100\%$ and the reaction cross section error as $\sigma_{r\varepsilon} = \varepsilon\sigma_r$. In our calculation, the statistical uncertainty of the reaction cross section is no more than 1.5%. We also perform the calculation of the reaction $O(^3P)+D_2 \rightarrow OD+D$ for collision energies of 1.0 and 1.5 eV (a batch of 50000 trajectories for each collision energy) and compared these with the results of $O(^3P)+H_2$ at the same collision energies. Since the two reactions at those two collision energies (1.0 and 1.5 eV) have relative high cross section values and scattering intensities, the comparison can be instructive.

The centre-of-mass (CM) frame is chosen such that the reactant relative velocity $\boldsymbol{k}$ is parallel to the z axis and the y axis is perpendicular to the xz-plane containing $\boldsymbol{k}$ and $\boldsymbol{k}'$ (the relative velocity of reaction product) vectors. θ_r and ϕ_r are the polar and the azimuthal angles of the final rotational angular momentum $\boldsymbol{j}'$. θ_t is the angle between $\boldsymbol{k}$ and $\boldsymbol{k}'$ (the so-called scattering angle). $\langle P_2(\boldsymbol{j}' \cdot \boldsymbol{k})\rangle$ is the rotational alignment parameter describing the degree of rotational alignment of the angular momentum $\boldsymbol{j}'$. $P(\theta_r)$ and $P(\phi_r)$ are probability density functions describing the probability density distribution of reaction products, reflecting $\boldsymbol{k} - \boldsymbol{j}'$ and $\boldsymbol{k} - \boldsymbol{k}' - \boldsymbol{j}'$ vector-correlation, respectively. A set of generalized polarization-dependent differential cross sections (PDDCSs) is used to describe the full three-dimensional angular distribution associated with $\boldsymbol{k} - \boldsymbol{k}' - \boldsymbol{j}'$ correlation in the CM frame, and they are $(2\pi/\sigma)(d\sigma_{00}/d\omega_t)$, $(2\pi/\sigma)(d\sigma_{20}/d\omega_t)$, $(2\pi/\sigma)(d\sigma_{22+}/d\omega_t)$, and $(2\pi/\sigma)(d\sigma_{21-}/d\omega_t)$ abbreviated as P_{00}, P_{20}, P_{22+}, and P_{21-}. The $\langle P_2(\boldsymbol{j}' \cdot \boldsymbol{k})\rangle$, $P(\theta_r)$, $P(\phi_r)$, and PDDCSs are detailed elsewhere[21,22,24,26]

The new surface reported by Brandão *et al.*[19] has different dynamical characteristics from those of Rogers *et al.*[18] The difference lies in the depth of the van der Waals region. The calculation of Brandão *et al.* demonstrates that the deeper van der Waals region in this surface can be interpreted to be a higher cross section than that of Rogers *et al.*'s surface, and it has been furthermore confirmed by our calculation.

3. Results and discussion

Figure 1 shows the calculated reaction cross sections each as a function of collision energy in comparison with other QCT[11] and quantum[5,13] calculations. The QCT result from Ref. [11] is calculated for the PES reported by Brandão *et al.*,[19] and the two quantum results are calculated on the ground $^3A''$ PES reported by Rogers *et al.*[18] Our results are consistent with the other calculations in an acceptable error range, confirming that our QCT calculations are reasonable and feasible. Figure 1 shows that the reaction cross section increases gradually with the increasing collision energy in the energy range investigated. In our study, we preset only the initial vibrational and rotational quantum states of the reagent H_2, and the product OH diatom does not have any specific quantum or electronic state. Our results can provide a good comparison with the calculations of Li and Han.[15]

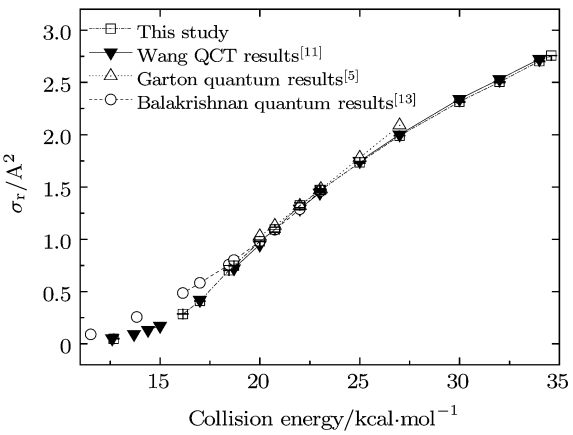


Fig. 1. Initial state-selected reaction cross sections for O (^{3}P)+H_2 ($\nu = 0$, $j = 0$) collisions on the $^3A''$ PES (1 cal=4.182 J).

$P(\phi_r)$ and $P(\theta_r)$ are both probability density functions describing the probability density distribution for a reaction product. Figure 2(a) shows a comparison among $P(\phi_r)$ distributions at different collision energies for the reaction $O(^3P)+H_2$. For this reaction only one peak appears at $\phi_r = 3\pi/2$. The peaks decrease in intensity as the collision energy increases. It is clear that the orientation of product OH is preferentially along the negative direction of the CM y-axis and the intensity decreases with increasing collision energy.

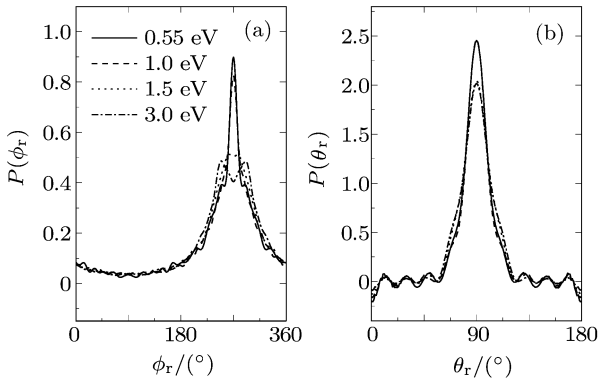


Fig. 2. Angular distributions of $P(\phi_r)$ and $P(\theta_r)$ at four collision energies of the O (^{3}P)+H_2 reaction. (a) $P(\phi_r)$ distribution shows the $\boldsymbol{k}-\boldsymbol{k}'-\boldsymbol{j}'$ vector correlations, (b) $P(\theta_r)$ describes the $\boldsymbol{k}-\boldsymbol{j}'$ correlation.

We also present a comparison among $P(\theta_r)$ distributions for various collision energies in Fig. 2(b). $P(\theta_r)$ reflects $\boldsymbol{k}-\boldsymbol{j}'$ vector correlation, namely the rotational alignment of the product. Figure 2(b) shows that the $P(\theta_r)$ distributions are relatively broad and symmetric, with peaks at $\theta_r = \pi/2$, which also demonstrates that the product rotational angular momentum vector prefers to be perpendicular to the initial relative velocity direction. It is clear in Fig. 2(b) that the peak and width of $P(\theta_r)$ generally decrease as collision energy increases. The $P(\theta_r)$ distributions at collision energies of 0.55 and 1.0 eV almost overlap and the other two distributions nearly overlap at a lower position in the plot. In Fig. 2(b), the rotational angular momentum of the product exhibits a type of forward stepwise variation to some extent.

The generalized PDDCSs describing $\boldsymbol{k}-\boldsymbol{k}'-\boldsymbol{j}'$ correlation and the scattering direction of the product molecule are presented in Fig. 3. The PDDCS P_{00}, which is proportional to the differential cross section (DCS), only describes the angular distribution of the product molecule and is not associated with the product orientation and alignment. It can be observed from Fig. 3(a) that the product OH molecules are strongly scattered backward at a collision energy of 0.55 eV. The OH molecules are scattered backward and sideways for collision energies of 1.0 and 1.5 eV. Different from the other three distributions, the PDDCS P_{00} at a collision energy of 3.0 eV indicates forward scattering of OH product molecules. The PDDCS P_{20}, which is the expectation value of the second Legendre moment $\langle P_2(\cos\theta_r)\rangle$, is shown in Fig. 3(b). The trajectory of P_{20} shows the opposite trend to that of P_{00}, which indicates the degree of alignment of the product rotational angular momentum $\boldsymbol{j}'$ perpendicular to $\boldsymbol{k}$. The P_{20} for a collision energy of 0.55 eV shows that $\boldsymbol{j}'$ is strongly aligned in the direction perpendicular to $\boldsymbol{k}$ in a scattering angle range of 90°–180°. The P_{20} distributions for collision energies of 1.0 and 1.5 eV show that the alignment of $\boldsymbol{j}'$ is much weaker than that for 0.55 eV, but the scattering angle range changes to 60°–180°. The alignment of $\boldsymbol{j}'$ for a collision energy of 3.0 eV is the weakest in the four trajectories, with weak alignment of $\boldsymbol{j}'$ perpendicular to $\boldsymbol{k}$ in the scattering angle range of 0°–135° and a downward peak at 54°. The PDDCS P_{20}, which indicates the alignment moment for rotation of product molecules, is related only to the PES and mass factor, i.e., $\cos^2\beta = m_A m_C/(m_A+m_B)(m_B+m_C)$ for the reaction A+BC→AB+C.[26] Since the reaction is fixed as specified in $O(^3P)+H_2$→OH+H, the one and only difference amongst the four P_{20} trajectories lies in collision energy. Suppose that the reaction between $O(^3P)$ and H_2 occurs on a three-dimensional surface (i.e., the potential surface), different collision energies can lead to different motion paths (i.e., reaction paths). We believe that the difference is mainly due to different motion paths on the PES arising from different collision energies.

At the extremities of backward and forward scattering, the polarization-dependent differential cross sections with $q \neq 0$ are equal to zero as shown in Figs. 3(c) and 3(d). Because the $\boldsymbol{k}-\boldsymbol{k}'$ scattering planes are not determined at these limiting scattering angles, the values of these polarization-dependent differential cross sections with $q \neq 0$ must be zero.[25] The representations of polarization-dependent differential cross sections with $q \neq 0$ for scattering away from the extreme forward and backward directions may be more attractive and can provide abundant dynamic information[25] about the ϕ_r dihedral angle distribution. In Fig. 3(c), it is clear that the values of P_{22+} are all negative for almost all scattering angles,

which indicates the remarkable preference for product alignment along the negative y-axis; the orientation of product along the positive y-axis is very weak as observed from the positive value of P_{22+} for part of the scattering angle range. The product exhibits unusual and quite a strong polarization at about 150° for a collision energy of 0.55 eV, and the degree of polarization is stronger than those for the other three collision energies. The degrees of polarization for 1.0 and 1.5 eV are similar and are weaker than the degree of polarization for 3.0 eV, although the positions are different for the different collision energies.

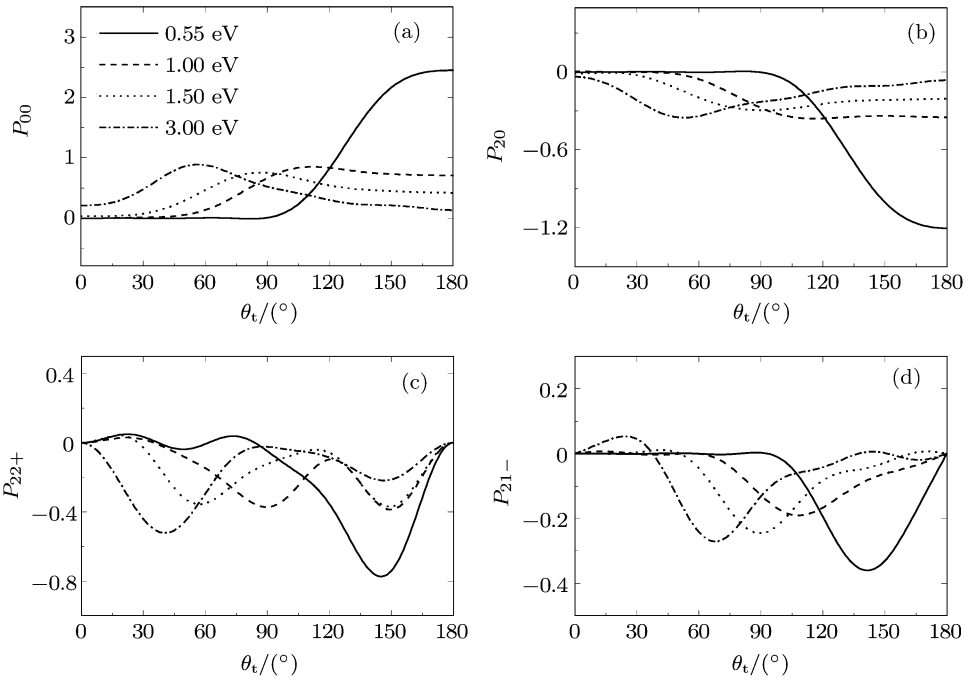


Fig. 3. Four polarized-dependent differential cross sections (PDDCSs) of the reaction O (^{3}P)+H_2 at four different collision energies: (a) $(k,q) = (0,0)$, (b) $(k,q\pm) = (2,0)$, (c) $(k,q\pm) = (2,2+)$, (d) $(k,q\pm) = (2,1-)$, respectively.

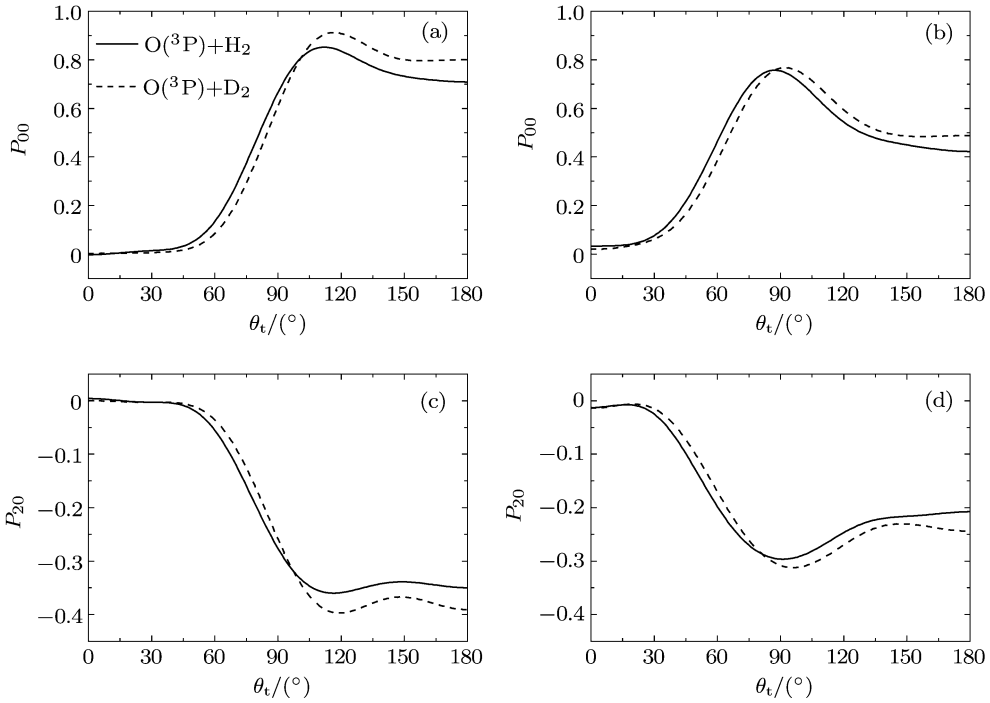


Fig. 4. Two PDDCSs of the reactions O (^{3}P)+H_2 and O (^{3}P)+D_2 at two collision energies: (a) the collision energy is 1.0 eV, $(k,q) = (0,0)$; (b) the collision energy is 1.5 eV, $(k,q) = (0,0)$; (c) the collision energy is 1.0 eV, $(k,q) = (2,0)$; (d) the collision energy is 1.5 eV, $(k,q) = (2,0)$.

The distributions of PDDCS P_{21-} are depicted in Fig. 3(d). The values are almost negative and close to zero, and show strong polarization for collision energies of 0.55–3.0 eV at approximately 140°, 110°, 90° and 70°. The degrees of polarization of P_{21-} for the four collision energies are also different.

To compare the two reactions, $O(^3P)+H_2 \rightarrow OH+H$ and $O(^3P)+D_2 \rightarrow OD+D$, on this PES, we also compute two PDDCSs with $(k,q) = (0,0)$ and $(2,0)$ for the $O(^3P)$ + D_2 reaction at collision energies of 1.0 and 1.5 eV, which are shown in Fig. 4. For the two collision energies, the degrees of forward scattering of the product molecules are stronger for $O(^3P)+D_2$ than for $O(^3P)+H_2$, although the difference is quite small. For the two collision energies, the degrees of product rotational alignment are stronger for $O(^3P)+D_2$ than for $O(^3P)+H_2$, but the difference is very limited.

We also calculate the rotational alignment parameters $\langle P_2(\boldsymbol{j}' \cdot \boldsymbol{k})\rangle$ to present the product rotational

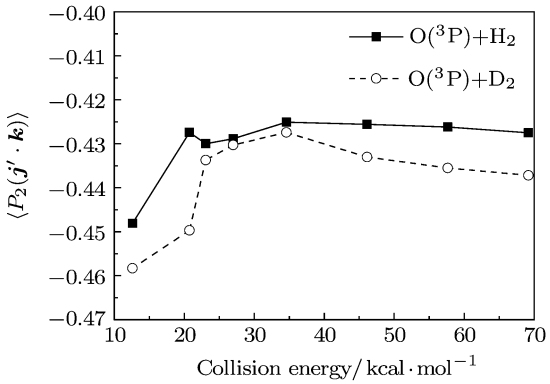


Fig. 5. Rotational alignment parameters $\langle P_2(\boldsymbol{j}' \cdot \boldsymbol{k})\rangle$ of product molecules of both the reactions $O(^3P) + H_2$ and $O(^3P) + D_2$.

alignment behaviour, and the results are shown in Fig. 5. The results show that the value of $\langle P_2(\boldsymbol{j}' \cdot \boldsymbol{k})\rangle$ is smaller for $O(^3P)+D_2$ than for $O(^3P)+H_2$, indicating that rotational alignment is stronger for the former than for the latter reaction. Although the effects of the mass factor in the two reactions are limited, the smaller the mass factor is, the stronger the product orientation and alignment are.

4. Conclusion

We calculate the product polarization for the reaction $O(^3P)+H_2$ using a QCT method. The PES for the $O(^3P)+H_2$ system in the lowest $^3A''$ state has been reported by Brandão *et al.*[19] The reaction cross section computed as a function of the collision energy is in perfect accordance with results computed using other methods.[5,11,13] On that basis, we calculate the vector correlations $P(\phi_r)$, $P(\theta_r)$ and the four generalized PDDCSs. We find that the product molecules show varying polarization behaviour as the collision energy changes. To compare the behaviours of $O(^3P)+H_2$ and $O(^3P)+D_2$ reactions, PDDCSs with $(k,q) = (0,0)$, (2,0), as well as the product rotational alignment parameters $\langle P_2(\boldsymbol{j}' \cdot \boldsymbol{k})\rangle$ for the reaction $O(^3P)+D_2$, are also calculated. We find that the mass factor slightly enhances the product orientation and alignment. Our calculations indicate that the polarization distribution of the product molecule exhibits different characteristics that can be ascribed to the different motion paths on the PES arising from various collision energies or the mass factor.

References

[1] Dixon-Lewis G and Williams D 1977 *J. Comput. Chem. Kinet.* **17** 1

[2] Reynard L M and Donaldson D J 2001 *Geophys. Res. Lett.* **28** 2157

[3] Presser N and Gordon R J 1985 *J. Chem. Phys.* **82** 1291

[4] Han J D, Chen X R and Weiner B R 2000 *Chem. Phys. Lett.* **332** 243

[5] Garton D J, Minton T K, Maiti B, Troya D and Schatz G C 2003 *J. Chem. Phys.* **118** 1585

[6] Koppea S, Laurenta T, Naikl P D, Volpp H R, Wolfruma J, Arusi-Parparb T, Barb I and Rosenwaksb S 1993 *Chem. Phys. Lett.* **214** 546

[7] Weck P F, Balakrishnan N, Brandão J, Rosa C and Wang W 2006 *J. Chem. Phys.* **124** 074308

[8] Garrett B C and Truhlar D G 1987 *Int. J. Quantum. Chem.* **31** 17

[9] Braunstein M, Adler-Golden S, Maiti B and Schatz G C 2004 *J. Chem. Phys.* **120** 4316

[10] Chu T S, Zhang X and Han K L 2005 *J. Chem. Phys.* **122** 214301

[11] Wang W L, Rosa C and Brandão J 2006 *Chem. Phys. Lett.* **418** 250

[12] Broida M and Persky A 1984 *J. Chem. Phys.* **80** 3687

[13] Balakrishnan N 2003 *J. Chem. Phys.* **119** 195

[14] Sultanov R A and Balakrishnan N 2004 *J. Chem. Phys.* **121** 11038

[15] Li B and Han K L 2009 *J. Phys. Chem.* A. **113** 10189

[16] Chatfield D C, Friedman R S, Lynch G C, Truhlar D G and Schwenke D W 1993 *J. Chem. Phys.* **98** 342

[17] Rassolov V A, Garashchuk S and Schatz G C 2006 *J. Phys. Chem.* A **110** 5530

[18] Rogers S, Wang D S, Kuppermann A and Walch S 2000 *J. Phys. Chem.* A **104** 2308

[19] Brandão J, Mogo C and Silva B C 2004 *J. Chem. Phys.* **121** 8861

[20] Luo W L, Wen R, Zhang L, Zhu Z H and Fu Y B 2009 *Chin. Phys.* B **18** 167
[21] Blais N C and Truhlar D G 1977 *J. Chem. Phys.* **67** 1540
[22] Han K L, He G Z and Lou N Q 1996 *J. Chem. Phys.* **105** 8699
[23] Xu Y, Zhao J, Yue D G, Liu H, Zheng X Y and Meng Q T 2009 *Chin. Phys.* B **18** 5308
[24] Shafer-Ray N E, Orr-Ewing A J and Zare R N 1995 *J. Phys. Chem.* **99** 7591
[25] Wang M L, Han K L and He G Z 1998 *J. Phys. Chem.* A **102** 10204
[26] Li R J, Han K L, Li F E, Lu R C, He G Z and Lou N Q 1994 *Chem. Phys. Lett.* **220** 281
[27] Zhang W Q, Cong S L, Zhang C H, Xu X S and Chen M D 2009 *J. Phys. Chem.* A **113** 4192
[28] Zhang W Q, Li Y Z, Xu X S and Chen M D 2010 *Chem. Phys.* **367** 115